Molecules and Cells

Therapeutic Potential of CKD-504, a Novel Selective Histone Deacetylase 6 Inhibitor, in a Zebrafish Model of Neuromuscular Junction Disorders

Hui Su Jeong[1], Hye Jin Kim[1], Deok-Ho Kim[2,3,4], Ki Wha Chung[5], Byung-Ok Choi[1,6,*], and Ji Eun Lee[1,7,*]

[1]Department of Health Sciences and Technology, Samsung Advanced Institute for Health Sciences & Technology, Sungkyunkwan University, Seoul 06351, Korea, [2]Department of Biomedical Engineering, Johns Hopkins University, Baltimore, MD 21205, USA, [3]Department of Neurology, Johns Hopkins University School of Medicine, Baltimore, MD 21205, USA, [4]Department of Medicine, Johns Hopkins University School of Medicine, Baltimore, MD 21205, USA, [5]Department of Biological Sciences, Kongju National University, Gongju 32588, Korea, [6]Department of Neurology, Samsung Medical Center, Sungkyunkwan University School of Medicine, Seoul 06351, Korea, [7]Samsung Biomedical Research Institute, Samsung Medical Center, Seoul 06351, Korea
*Correspondence: bochoi77@hanmail.net (BOC); jieun.lee@skku.edu (JEL)
https://doi.org/10.14348/molcells.2022.5005
www.molcells.org

The neuromuscular junction (NMJ), which is a synapse for signal transmission from motor neurons to muscle cells, has emerged as an important region because of its association with several peripheral neuropathies. In particular, mutations in *GARS* that affect the formation of NMJ result in Charcot-Marie-Tooth disease and distal hereditary motor neuropathy. These disorders are mainly considered to be caused by neuronal axon abnormalities; however, no treatment is currently available. Therefore, in order to determine whether the NMJ could be targeted to treat neurodegenerative disorders, we investigated the NMJ recovery effect of HDAC6 inhibitors, which have been used in the treatment of several peripheral neuropathies. In the present study, we demonstrated that HDAC6 inhibition was sufficient to enhance movement by restoring NMJ impairments observed in a zebrafish disease model. We found that CKD-504, a novel HDAC6 inhibitor, was effective in repairing NMJ defects, suggesting that treatment of neurodegenerative diseases via NMJ targeting is possible.

Keywords: CKD-504, GARS, HDAC6 inhibitor, neuromuscular junction, zebrafish

INTRODUCTION

The neuromuscular junction (NMJ) is a chemical synapse established by motor neurons in the spinal cord and muscle fibers in the peripheral nervous system (PNS). In the NMJ, the presynaptic axons of motor neurons release acetylcholine, which binds to acetylcholine receptors (AChRs) present on the surface of the postsynaptic muscle fibers. Thus, the NMJ is important for transmitting neuronal signals to innervated muscles involved in peripheral movements. Impairments in the NMJ lead to muscle weakness due to disrupted neuronal transmission, which results in several diseases, such as Lambert-Eaton syndrome (presynaptic) and myasthenia gravis (postsynaptic) (Howard, 2018; Kesner et al., 2018; Rodriguez Cruz et al., 2020).

Among peripheral neuropathies, Charcot–Marie–Tooth (CMT) disease is one of the most commonly inherited neuropathies in both sexes and all ethnic groups (Morena et al., 2019). The disease includes numerous subtypes (types 1-7 and X-linked forms), with common symptoms of progressive muscle weakness and atrophy in the early stage and deformities of the foot and hand in the late stage (Morena et al., 2019). CMT type 2 is common, and most causative genes are

Received 11 October, 2021; revised 19 December, 2021; accepted 25 December, 2021; published online 30 March, 2022

eISSN: 0219-1032

mainly involved in the axonal development of motor neurons (Borg and Ericson-Gripenstedt, 2002; Loprest et al., 1992). CMT type 2D results from mutations in *GARS*, which encodes the ubiquitous enzyme glycyl-tRNA synthetase (GlyRS) and is associated with synaptic transmission at the NMJ (Antonellis et al., 2003; 2006; Lee et al., 2012; Sleigh et al., 2014). Several studies have reported that most mutations in *GARS* identified in CMT type 2D, including L129P, G240R, E71G, and H418R, result in muscle atrophy and weakness (Sivakumar et al., 2005). In a recent study, additional mutations in *GARS* (D200N and S265F) were identified in distal hereditary motor neuropathy type 5 (dHMN5) (Lee et al., 2012), and these mutations appeared to be associated with neuronal degeneration and weakened synaptic transmissions (Lee et al., 2012; Niehues et al., 2015).

Notably, several cases of *Gars*-mutant mice showed overt NMJ dysfunction (Seburn et al., 2006) combined with neuronal defects (Sleigh et al., 2017). Accordingly, it has been suggested that the pathophysiology of CMT type 2D is associated with the role of GARS as it interacts with neuropilin-1 at the neuronal terminal of the NMJ and modulates vascular endothelial growth factor signaling, thereby regulating neuronal axon guidance and muscle innervation (He et al., 2015). Although the NMJ has been shown to have a potential association with disease mechanisms of peripheral neuropathy, including CMT and dHMN5, effective NMJ- or GARS-targeted therapy has not been explored for this disorder.

In contrast, mutations in *GARS* have been reported to result in aberrant interactions with histone deacetylase type 6 (HDAC6), thereby increasing microtubule deacetylation (Mo et al., 2018). In addition, *Gars*-mutant mice showed a decrease in acetylated α-tubulin due to hyperactivated HDAC6, which disrupts axonal transport of motor proteins (Chen et al., 2010). Thus, HDAC6 inhibitors have emerged as promising treatments for several types of peripheral neuropathy (Benoy et al., 2018). In particular, an HDAC6 inhibitor restored the tubulin-involved axonal transport defects in a mouse model of CMT type 2 (d'Ydewalle et al., 2011). These studies suggest the potential importance of GARS-dependent HDAC6 inactivation in regulating NMJ formation and function. However, the pathophysiology of NMJ disorders remains poorly understood.

In this study, we investigated the efficacy of HDAC6 inhibition in repairing NMJ defects in peripheral neuropathies. We first generated an NMJ disease model using zebrafish (*Danio rerio*), which is generally used for drug screening, as well as for modeling peripheral neuropathies such as CMT (Cirrincione and Rieger, 2020; Ennerfelt et al., 2019; Ponomareva et al., 2016). We investigated the effects of several HDAC6 inhibitors on recovery from NMJ defects, including muscle dysfunction. We found that HDAC6 inhibitors significantly restored NMJ innervation and motility in zebrafish. In addition, we demonstrated the efficacy of a novel HDAC6 inhibitor, CKD-504, in repairing malformations and dysfunction of NMJs in a zebrafish disease model. Therefore, our results suggest that the novel HDAC6 inhibitor CKD-504 could be a potential therapeutic approach for NMJ diseases such as CMT and dHMN5.

MATERIALS AND METHODS

Zebrafish housing and manipulations

Adult zebrafish were maintained with a cycle of 13-h light and 11-h dark in an automatic system (Genomic-Design, Korea) at 28.5°C and pH of 7.0-7.9. The zebrafish embryos were collected via natural breeding and incubated in clean petri dishes containing E3 medium (297.7 mM NaCl, 10.7 mM KCl, 26.1 mM $CaCl_2$, and 24.1 mM $MgCl_2$), with 1% methylene blue (M2662; Samchun Chemicals, Korea), at 28.5°C. To inhibit the production of melanin, which interferes with immunostaining, zebrafish larvae were raised in E3 medium containing 0.2 mM N-phenylthiourea (P7629; Sigma-Aldrich, USA). Animal research was reviewed and approved by the Institutional Animal Care and Use Committee of Samsung Biomedical Research Institute/Samsung Medical Center and Sungkyunkwan University (IACUC#20201008001 and IACUC#20200916001).

Microinjection into zebrafish

To block the expression of zebrafish *gars*, splice-blocking antisense MOs, 5'-GGGCCTGGAGGCAACATGCA-3', were designed and synthesized by GeneTools (USA). The MOs were dissolved in nuclease-free water and 2.5 ng of MOs were microinjected into zebrafish embryos at the 1-2 cell stage using a gas-powered microinjection system (PV83 Pneumatic PicoPump, SYS-PV830; World Precision Instruments, USA). The capped mRNAs of the human gene (wild-type [WT] *GARS*) were subcloned into the pCS2+ vector and then synthesized using the mMESSAGE mMACHIN SP6 kit (AM1340; Ambion, USA). *In vitro*-synthesized mRNAs (1,000-1,500 pg) were injected into zebrafish embryos with *gars* MOs.

Immunohistochemistry

Zebrafish larvae at 84 h post-fertilization (hpf) were fixed in 4% paraformaldehyde in 0.1 M phosphate-buffered saline (PBS) at 4°C overnight. The fixed zebrafish larvae were permeabilized with PBST (0.5% TritonX-100 in 0.1 M PBS) for 15 min. The larvae were then washed with 1× PBS three times and blocked in PBDT (1% DMSO and 1% BSA in PBST) containing 4% normal goat serum at room temperature for 1 h. The larvae were incubated with the following primary antibodies: mouse anti-SV2 (1:50; Developmental Studies Hybridoma Bank, USA) and Alexa 647-conjugated α-BTX (B35450, 1:150; Molecular Probes, USA) antibodies at 4°C overnight in blocking solution. After washing three times with PBST, the larvae were incubated with Alexa Fluor 488-conjugated secondary antibodies (mouse A11001, 1:250; Life Technologies, USA) at RT for 2 h. The larvae were mounted on slides with PBS containing 70% glycerol. To generate imaging data, the mounted larvae were imaged using a confocal microscope (LSM 700; Carl Zeiss, Germany) and analyzed using ImageJ (NIH, USA) or Zeiss ZEN imaging software. The formed presynapse, postsynapse, and NMJ were analyzed by measuring the proportion of areas with green, red, and merged yellow signals within the region of interest (ROI) of the zebrafish trunk, respectively. To assess the extent of NMJ innervation, the proportion of areas with yellow signals within each area of green and red signals was measured.

Immunoblot assay

At 3 days post-fertilization (dpf), zebrafish larvae were washed with PBS and lysed with T-per tissue protein extraction buffer (78510; Thermo Scientific, USA). Protein samples (30 μg) were denatured at 100°C for 5 min, and then separated using SDS-PAGE. The proteins were transferred onto a 0.45 μm PVDF membrane (IPVH00010; Millipore, USA), and the membrane was immersed in a blocking solution (TBST [Tris-buffered saline pH 7.5, containing 0.5% Tween-20] containing 5% skim milk [232100; BD Biosciences, USA]) at room temperature. The membranes were then incubated with the following primary antibodies overnight at 4°C: anti-GARS (sc-365442; Santa Cruz Biotechnology, USA), anti-HDAC6 (07-732; Millipore), anti-acetylated tubulin (T7451; Sigma-Aldrich), and anti-β-actin (sc-47778; Santa Cruz Biotechnology). The membranes were washed three times with TBST buffer and incubated with secondary antibodies for 1 h at room temperature. Finally, the membrane was enhanced with a chemiluminescence substrate (NEL104001EA; PerkinElmer, USA) to visualize the specific proteins. The expression level of each protein was normalized to that of β-actin in each blot and quantified using ImageJ.

Zebrafish motility analysis

The velocities of the zebrafish larvae were analyzed using light stimulation using with DanioVision (Noldus, Netherlands). Individual larvae injected with MOs or mRNAs were transferred onto 24-well plates, with each well containing 1 ml of E3 medium. The movements of the larvae that responded to light were recorded for 30 min and analyzed using EthoVision XT software (Noldus).

Drug/chemical treatment

All drugs and chemicals tested in this study were used twice in zebrafish at 48 and 72 hpf until fixation at 84 hpf. Vorinostat and pomiferin, selected from the Pharmakon-1760 collection (MicroSource Discovery Systems, USA), were dissolved in DMSO and used at a concentration of 10 μM in larvae submerged in E3 media. Tubastatin A and CKD-504 were dissolved in distilled water and used at a concentration of 20 μM.

Statistical analysis

All statistical analyses were performed using GraphPad Prism 5 (GraphPad Software, USA). Values are presented as mean ± SD or fold change relative to the mean control. Differences between two groups were evaluated using unpaired Student's *t*-test, and differences among multiple groups were analyzed using one-way ANOVA with Tukey's post hoc test. A P value of <0.05 was considered statistically significant for any statistical test. All quantifications for statistical analyses were performed using double-blind tests.

RESULTS

Generation of an NMJ disease model by knocking-down *gars* in zebrafish

The zebrafish was used to model peripheral neuropathy with NMJ defects *in vivo*. The zebrafish is an efficient vertebrate model to study neurological disorder mechanisms and is useful for drug screening (Bremer et al., 2017; Chapela et al., 2019; Cirrincione et al., 2020). To knock down *gars* that is mutated in CMT type 2, we designed splice-blocking morpholino oligonucleotides (MOs) (Jung et al., 2020) targeting exon 7 of zebrafish *gars* (Fig. 1A). At 5 dpf, zebrafish embryos injected with *gars* MOs (2.5 ng/nl) were developmentally normal, but very few embryos showed morphological defects such as a curved body, small brain, and yolk dilatation (Figs. 1B and 1C). Quantitative reverse transcription polymerase chain reaction (RT-PCR) analysis confirmed that the embryos injected with *gars* MOs produced an alternative splicing form of *gars* (Fig. 1D), which was not present in zebrafish embryos injected with control MOs. In addition, we showed that *gars*-knocked down (*gars*-KD) zebrafish produced significantly less gars protein than controls using immunoblot analysis (Figs. 1E and 1F). These data suggest that the designed splice-blocking MOs were sufficient to deplete zebrafish *gars*, but *gars*-KD zebrafish exhibit few morphological defects during development.

Next, to determine whether the deficit of *gars* affects the development of NMJs *in vivo*, we performed immunohistochemistry on the trunks of MOs-injected zebrafish (Fig. 2A). NMJs are formed after synaptic innervation and muscle maturation in the PNS, and mature after signal transmission from motor neurons to muscle fibers in zebrafish at 3 dpf (Menelaou et al., 2008). Thus, we stained NMJs with anti-SV2 antibodies to mark presynaptic vesicles from motor neurons and α-bungarotoxin (α-BTX) to mark postsynaptic AChRs on muscle fibers in 84 hpf larvae. The effect of gars on NMJ development was analyzed by comparing the NMJ area, indicated by a yellow signal within the ROI, between control MOs- and *gars* MOs-injected larvae (Fig. 2B). The *gars*-KD larvae had fewer NMJs than the control larvae, implying an important role for *gars* in NMJ formation. We further analyzed the extent of NMJ innervation by comparing each signal labeled with pre- or postsynaptic markers in the putative NMJ areas of MO-injected larvae (Figs. 2C-2I) with those of control MOs-injected larvae. The *gars*-KD larvae had fewer yellow signals than the control larvae in the presynaptic (Figs. 2E and 2H) and postsynaptic (Figs. 2F and 2I) regions of the NMJ. In addition, to ascertain that the NMJ defects observed in *gars*-KD zebrafish were not due to an overall developmental defect or delay following *gars* silencing, we analyzed the effect of *gars* depletion on brain development, rather than the PNS. At both 84 hpf and 120 hpf, the *gars*-KD zebrafish exhibited no significant morphological defects in the brain (Supplementary Figs. S1A and S1B). We also confirmed that *gars* depletion had little effect on brain size (Supplementary Figs. S1C and S1D), but caused defects in NMJ innervation even at 120 hpf (Supplementary Figs. S1E-S1G). These results suggest that gars is essential for the initial development of NMJs.

Role of GARS in NMJ development is evolutionarily conserved

Based on the identification of mutations in *GARS* from distal motor neuropathies, including CMT type 2D and dHMN5 (Lee et al., 2012), we examined whether human GARS

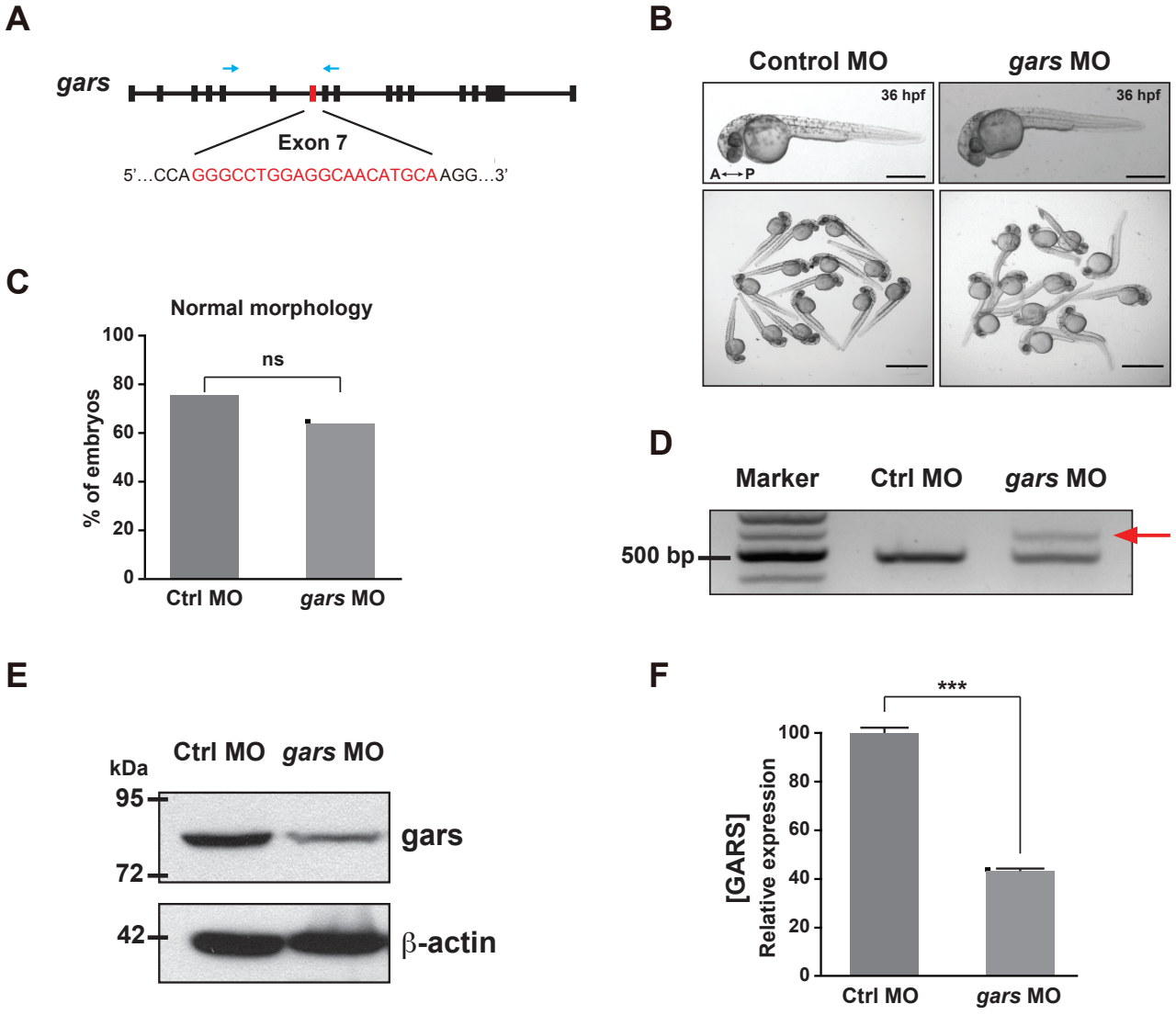

Fig. 1. Generation of the *gars*-KD zebrafish model. (A) Schematic of the target of the designed splicing-blocking morpholino oligos (MOs) on exon 7, targeting the zebrafish *gars* gene (red letters). Blue arrows indicate the targets of the primers used for RT-PCR shown in (D). (B) Images showing morphologies of control MOs- or *gars* MOs-injected larvae at 36 hpf. A, anterior; P, posterior. Scale bars = 500 μm (individual images); 2,000 μm (group images). (C) Quantification of zebrafish embryos showing morphological phenotypes, counted in each genotype at 5 dpf. Statistical significance was determined using unpaired Student's *t*-test. ns, non-significant. (D) RT-PCR results confirming *gars* splicing on exon 7. A red arrow indicates an alternative splicing form induced by *gars* MOs. (E and F) Comparison of zebrafish gars expression between control and *gars* KD zebrafish. Results of immunoblot assays for gars and β-actin (E). Protein levels were normalized against β-actin in the same blots, and the quantification of *gars* expression is presented graphically in (F). Statistical significance was determined using unpaired Student's *t*-test. $***P < 0.001$.

played a role in the recovery of NMJ defects in the zebrafish model. We generated mRNA from DNA constructs of the human WT *GARS*. We then introduced the mRNAs exogenously into *gars*-KD zebrafish embryos and observed the effect of exogenous human *GARS* expression on NMJ impairment in zebrafish larvae. Disrupted NMJ formation in *gars*-KD larvae was restored by exogenous human WT *GARS* (Figs. 3A and 3B). Furthermore, we compared the extent of NMJs in each presynaptic and postsynaptic ROI between zebrafish larvae that did and did not express WT *GARS*. The reduced yellow signals present in both pre- and postsynaptic NMJ regions of the *gars*-KD larvae were recovered following exogenous expression of human WT *GARS* (Figs. 3C-3G). Taken together, these results suggest that the function of GARS in the regulation of NMJ development is evolutionarily conserved.

Silencing of *gars* affects the motility of zebrafish

To clarify whether GARS-mediated NMJ development is involved in peripheral neuropathology, we investigated the effects of *gars* depletion on the movement of zebrafish lar-

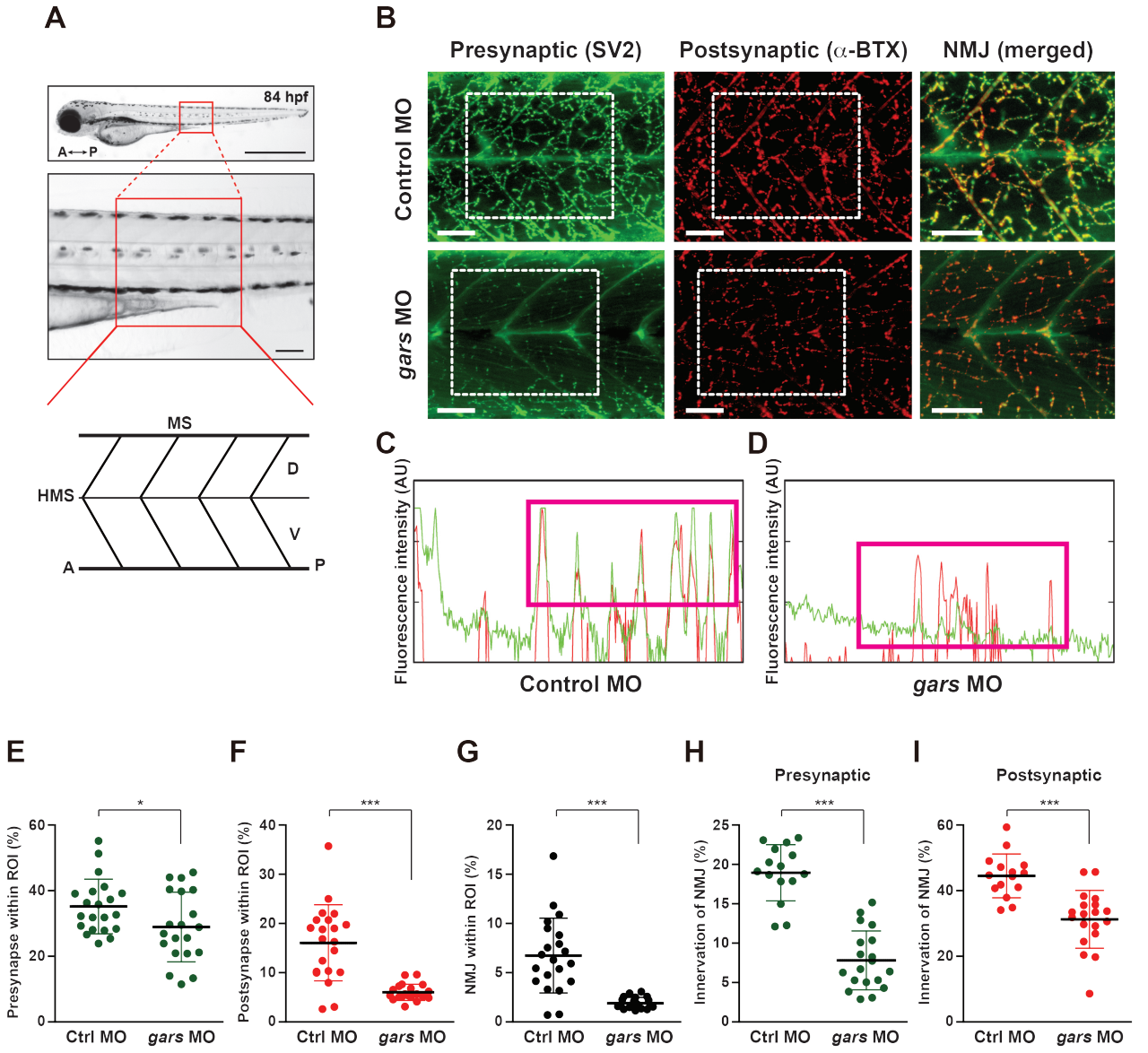

Fig. 2. Depletion of *gars* results in anomalies in the NMJ in zebrafish larvae. (A) Schematic showing the representative region where NMJs in the larval trunks were analyzed and observed. A, anterior; P, posterior; HMS, horizontal myoseptum; MS, myosepta; D, dorsal; V, ventral. Scale bars = 1,000 μm (top images) and 50 μm (bottom images). (B) Lateral view images after staining with anti-SV2 (presynaptic region) and α-BTX (postsynaptic region) of the whole-mounted larva injected with control or *gars* MOs at 84 hpf. Merged images (NMJ) are magnified from the images in the rectangular regions. Scale bars = 50 μm. (C and D) Comparison of fluorescence intensity (a.u.) (green, presynapse; red, postsynapse) between control MOs- (C) and *gars* MOs-injected (D) zebrafish embryos. (E-G) Comparisons of presynapse (E), postsynapse (F), and NMJ (G) signal ratios within the region of interest (ROI) between control MOs- (n = 21) and *gars* MOs-injected (n = 20) zebrafish embryos. Statistical significance was determined using unpaired Student's *t*-test. $*P < 0.05$; $***P < 0.001$. (H and I) Comparisons of NMJ innervation in the presynaptic area (H) and postsynaptic (I) areas between control MOs- (n = 15) and *gars* MOs-injected (n = 19) zebrafish embryos. Statistical significance was determined using unpaired Student's *t*-test. $***P < 0.001$.

vae. Using a zebrafish-specific behavior analysis system, we first monitored the swimming velocity of control and *gars* MOs-injected larvae at 5 dpf. The zebrafish larvae were individually placed into 24-well plates containing embryo media, and their movement was recorded for 30 min under light and then analyzed (Fig. 4A). The heatmap tracking data of the moving pattern of each zebrafish larva revealed that the *gars*-KD larvae were less motile than control larvae (Fig. 4B). The swimming velocity of each zebrafish larva was calculated by measuring the total distance traveled during the recording time. The results showed that the moving velocity of *gars*-KD larvae was lower than that of control larvae (Fig. 4C). We further tested the effects of human *GARS* on the swimming velocity of *gars*-KD zebrafish larvae. Zebrafish expressing ex-

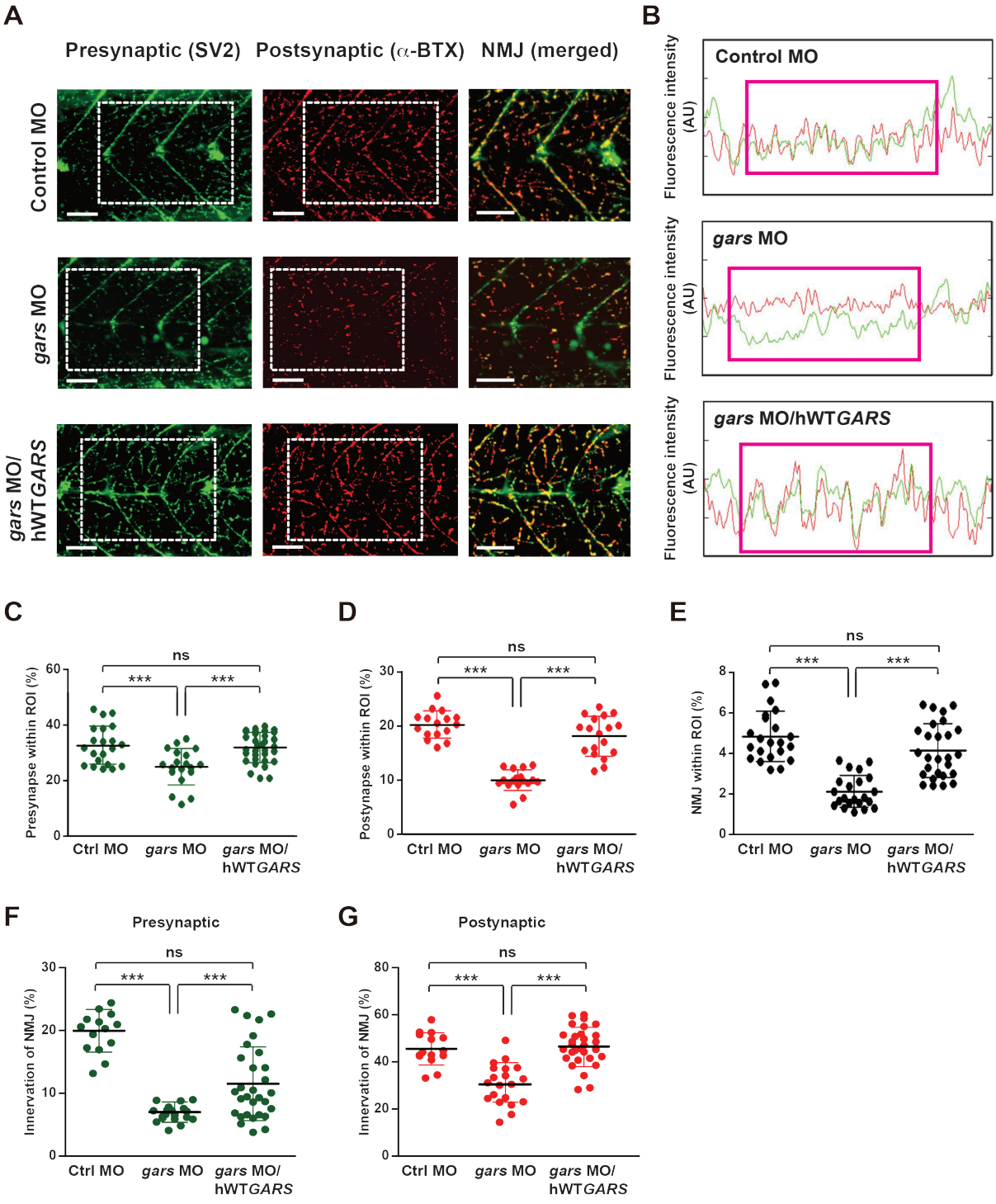

Fig. 3. Overexpression of human *GARS* restores NMJ defects in zebrafish. (A) Lateral view images after staining with anti-SV2 and α-BTX of the whole-mounted zebrafish injected with control, *gars* MOs, and human WT mRNA at 84 hpf. The merged images (NMJs) are magnified from the images in the rectangular regions. Scale bars = 50 μm. (B) Comparisons of fluorescence intensity (green, presynapse; red, postsynapse) among MOs and mRNAs injected zebrafish embryos. (C-E) Comparison of presynapse (C), postsynapse (D), and NMJ (E) signal ratios within the ROI among zebrafish embryos injected with control MOs (n = 22), *gars* MOs (n = 22), and *gars* MOs with WT (n = 33) mRNAs. Statistical significance was assessed using one-way ANOVA followed by Tukey's post hoc test. ***$P < 0.001$. ns, non-significant. (F and G) Comparison of NMJ innervation in the presynaptic area (F) and postsynaptic area (G) among zebrafish embryos injected with control MOs (n = 15), *gars* MOs (n = 19), and *gars* MOs with human WT *GARS* mRNAs (n = 30). Statistical significance was determined using one-way ANOVA followed by Tukey's post hoc test. ***$P < 0.001$. ns, non-significant.

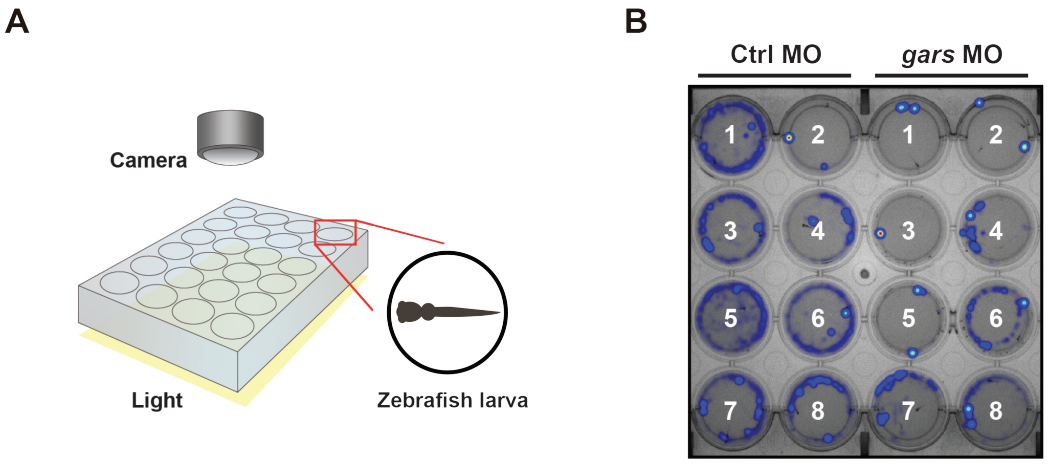

Fig. 4. *gars*-KD zebrafish larvae have low motility. (A) Simplified diagram showing how to use the DanioVision system to analyze zebrafish behaviors that occur when they respond to light stimulation. (B) Heatmap images comparing swimming patterns between control and *gars* MOs-injected larvae recorded for 30 min. (C) Quantification of velocity measured in zebrafish larvae injected with control MOs (n = 57), *gars* MOs (n = 47), and *gars* MOs with human WT *GARS* (n = 56) mRNAs. Statistical significance was assessed using one-way ANOVA followed by Tukey's post hoc test. $*P < 0.05$; $***P < 0.001$. ns, non-significant.

ogenous human WT *GARS* showed significant rescue of motility deficits (Fig. 4C). Taken together, these data, including those in Fig. 3, suggest that GARS-mediated NMJ function is important for controlling peripheral movement.

Inhibition of HDAC6 is important for repairing NMJ defects

Previous studies have reported that mutant forms of *GARS* induce tubulin deacetylation by interacting with HDAC6 (Mo et al., 2018), and the application of HDAC6 inhibitors is effective for the recovery of peripheral neuropathy (Benoy et al., 2018). Hence, we hypothesized that the inhibition of HDAC6 could repair NMJ defects by knocking down *gars* in zebrafish larvae. We confirmed that depletion of *gars* in zebrafish increased the deacetylation levels of α-tubulin without significantly affecting the expression of HDAC6 (Supplementary Figs. S2A and S2B). Furthermore, we revealed that exogenously expressed GARS restored the acetylation of α-tubulin in a dose-dependent manner in *gars*-KD zebrafish (Supplementary Figs. S2C and S2D). These data indicate the importance of GARS in controlling α-tubulin (de)acetylation in the NMJ. Next, we examined the effects of tubastatin A, a potent and selective HDAC6 inhibitor (Butler et al., 2010) on damaged NMJs. We treated 48 hpf control and *gars* MOs-injected larvae twice with 20 μM of tubastatin A within 36 h. Immunostaining with anti-SV2 antibodies and α-BTX revealed that treatment with tubastatin A restored the NMJ anomaly induced by *gars* depletion (Figs. 5A and 5B). We also quantified the extent of NMJ innervation in the putative NMJ region of tubastatin A-treated larvae and compared it with that of *gars*-KD larvae. The results revealed that the reduced fluorescence signals observed in both the presynapse and postsynapse of the NMJ in *gars* MOs-injected zebrafish were significantly restored by tubastatin A (Figs. 5C-5G). Furthermore, we found that the motility of *gars*-KD larvae was restored to the same level as that of the control larvae after treatment with tubastatin A (Supplementary Fig. S3). Therefore, these data suggest that HDAC6 inhibition is involved in recovering the defects of NMJs and in evolutionarily conserved normal development.

CKD-504 is a novel HDAC6 inhibitor effective in restoring impaired NMJs

To elucidate the efficacy of HDAC6 inhibitors as potential treatments for NMJ disorders, we focused on U.S. Food and Drug Administration (FDA)-approved drugs that have been used to treat cancers, but not peripheral neuropathies. We

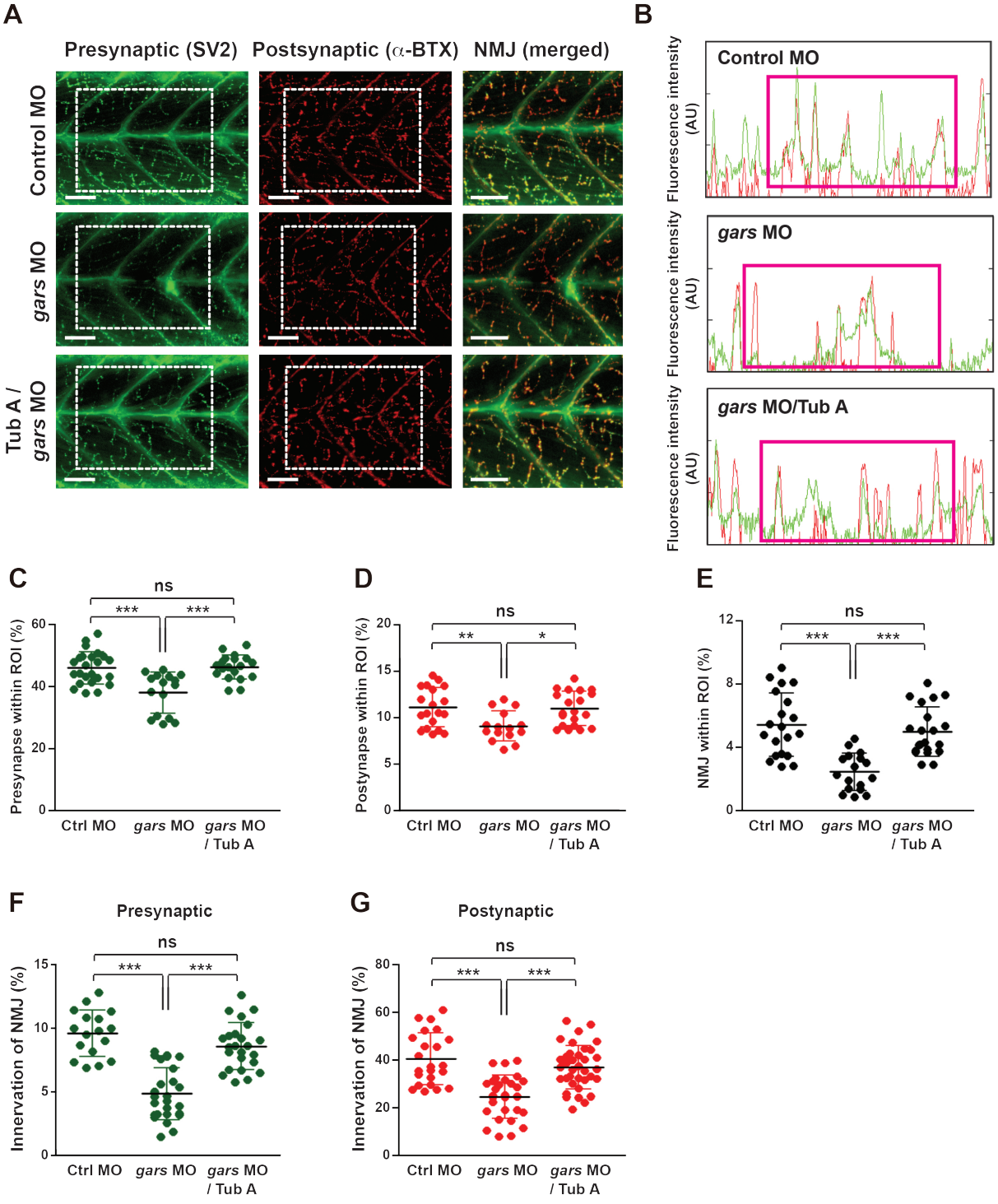

Fig. 5. Impaired NMJs can be restored by inhibiting HDAC6. (A) Lateral view images after staining with anti-SV2 and α-BTX of a whole-mounted zebrafish injected with control, *gars* MOs, or treated with tubastatin A (TubA). The merged images are magnified from the images in the rectangular regions. Scale bars = 50 μm. (B) Comparison of fluorescence intensity (green, presynapse; red, postsynapse) among MO-injected and TubA-treated zebrafish embryos. (C-E) Comparison of presynapse (C), postsynapse (D), and NMJ (E) signal ratios within the ROI among zebrafish embryos injected with control MOs (n = 24), *gars* MOs (n = 17), and *gars* MOs with TubA (n = 21). Statistical significance was assessed using one-way ANOVA followed by Tukey's post hoc test. $*P < 0.05$; $**P < 0.01$; $***P < 0.001$. ns, non-significant. (F and G) Comparison of NMJ innervation in the presynaptic (F) and postsynaptic (G) areas among zebrafish embryos injected with control MOs (n = 23), *gars* MOs (n = 29), and *gars* MOs with a TubA treatment (n = 36). Statistical significance was determined using one-way ANOVA followed by Tukey's post hoc test. $***P < 0.001$. ns, non-significant.

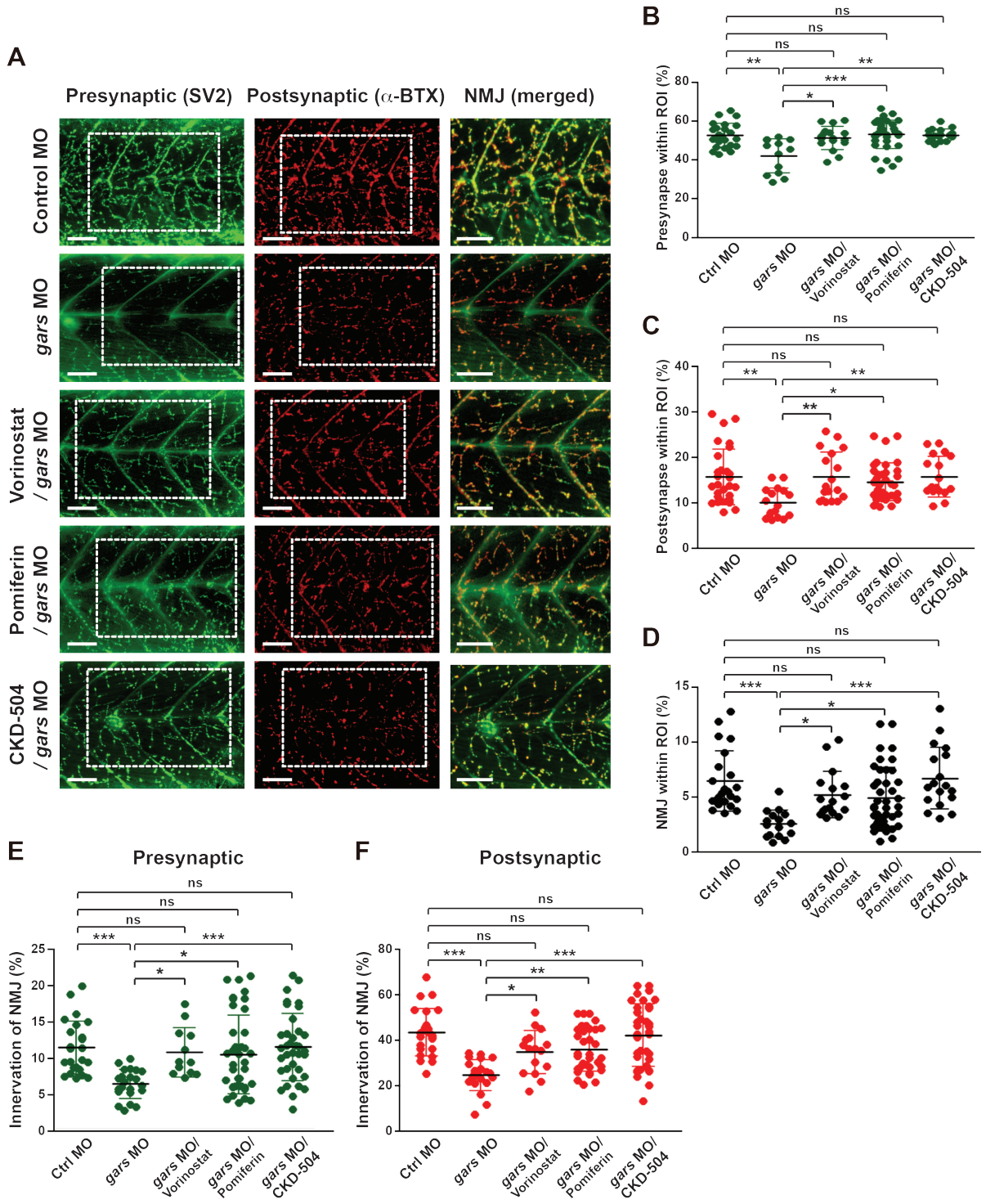

Fig. 6. CKD-504 is an efficient HDAC6 inhibitor that repairs NMJ defects. (A) Lateral view images after staining with anti-SV2 and α-BTX of a whole-mounted zebrafish injected with control or *gars* MOs, or treated with CKD-504 or FDA-approved drugs. The merged images are magnified from the images in the rectangular regions. Scale bars = 50 μm. (B-D) Comparisons of presynapse (B), postsynapse (C), and NMJ (D) signal ratios within the ROI among zebrafish embryos injected with control MOs (n = 29), *gars* MOs (n = 17), *gars* MOs with vorinostat (n = 18), pomiferin (n = 41), or CKD-504 (n = 18). Statistical significance was assessed using one-way ANOVA followed by Tukey's post hoc test. $*P < 0.05$; $**P < 0.01$; $***P < 0.001$. ns, non-significant. (E and F) Comparison of NMJ innervation in the presynaptic area (E) and postsynaptic (F) areas among zebrafish embryos injected with control MOs (n = 24); *gars* MOs (n = 22); and *gars* MOs with vorinostat (n = 16), pomiferin (n = 36), and CKD-504 (n = 36). Statistical significance was determined using one-way ANOVA followed by Tukey's post hoc test. $*P < 0.05$; $**P < 0.01$; $***P < 0.001$. ns, non-significant.

considered two different drugs, vorinostat and pomiferin, that inhibit HDACs, including HDAC6, in cancer (Licciardi and Karagiannis, 2012; Mariadason, 2008; Namdar et al., 2010). Vorinostat is the first FDA-approved treatment for cutaneous T-cell lymphoma with HDAC6 inhibitory activity (Mann et al., 2007). In contrast, pomiferin is a novel HDAC inhibitor isolated from flavonoid compounds (Son et al., 2007) and has been proven to be effective in inhibiting the growth of colon cancer cells (Mariadason, 2008; Son et al., 2007). We investigated the therapeutic effects of vorinostat and pomiferin on the impaired NMJs of *gars*-KD larvae. Immunostaining data and behavioral analysis showed that the NMJ defects in *gars*-KD larvae were repaired following treatment with 10 μM vorinostat and pomiferin (Fig. 6A, Supplementary Fig. S3B).

A recently reported novel HDAC6 inhibitor, CKD-504, which specifically affects the acetylation of α-tubulin (Choi et al., 2020), is effective in treating not only PNS disorders (e.g., CMT type 1A) but also in CNS disorders (e.g., Alzheimer's disease) (Choi et al., 2020; Ha et al., 2020). Hence, as compared with vorinostat and pomiferin, we determined whether CKD-504 could lead to recovery from NMJ diseases, such as CMT type 2D, by influencing the GARS-related NMJ formation. We injected *gars* MOs into zebrafish embryos and treated them twice with 20 μM CKD-504 at 48 hpf within 36 h. We then observed the extent of NMJ recovery by immunostaining with an anti-SV2 antibody, α-BTX, and analyzed motility. We found that innervations of NMJs in both presynaptic and postsynaptic regions were remarkably restored in CKD-504-treated larvae compared with those treated with other HDAC inhibitors, including tubastatin A, vorinostat, and pomiferin (Figs. 6B-6F). In addition, we found that motility deficits of *gars*-KO larvae were significantly restored after CKD-504 treatment (Supplementary Fig. S3). Taken together, these results suggest that the HDAC6-selective inhibitor CKD-504 as well as pan-HDAC inhibitors, vorinostat and pomiferin, are effective in repairing NMJ defects and may be a potential treatment for NMJ diseases, including CMT type 2D.

DISCUSSION

Here, we hypothesize that HDAC6 inhibition is key in repairing NMJ damage associated with peripheral neuropathies, including CMTs. We demonstrated that a novel HDAC6 inhibitor, CKD-504, is effective in restoring NMJ deficits in zebrafish larvae lacking *gars* and plays an important role in NMJ development and function (Grice et al., 2015; Sleigh et al., 2014). We also found that tubastatin A and FDA-approved drugs that inhibit HDACs repaired NMJ defects caused by *gars* deficiency. Notably, we showed that the recovery of NMJs because of HDAC6 inhibition was sufficient to prevent peripheral motility defects. Thus, these data suggest that HDAC6 inhibitors, especially CKD-504, could be used as potential treatments for NMJ-related disorders, including CMTs.

Posttranslational modifications (PTMs) of microtubules, such as acetylation, detyrosination, polyglutamylation, and polyglycylation, are important for the regulation of microtubule polymerization and depolymerization, which are major determinants of microtubule stability (Janke and Bulinski, 2011). In particular, (de)acetylation of Lys40 of α-tubulin in the lumen of microtubules is modulated by α-tubulin acetyltransferase (αTAT) and HDAC6 (Asthana et al., 2013; Kalebic et al., 2013; Zhang et al., 2003). The reciprocal function of αTAT and HDAC6 is also associated with several signaling pathways, such as Rho/ROCK signaling, that regulate axonal growth through the cytoskeletal network (Wong et al., 2018). Previous reports have shown that HDAC6 inhibition in neurodegenerative diseases leads to an increase in microtubule acetylation, which improves neurite growth, axonal transportation, neuroprotection, and mitochondrial movements (Simoes-Pires et al., 2013; Wenzel et al., 2019). It is noteworthy that HDAC6 inhibition was involved not only in enhancing NMJ stability but also in the clustering of AChRs on the postsynaptic side of the NMJ (Osseni et al., 2020; Smith et al., 2022). Correspondingly, our data clearly showed that *gars* depletion-induced NMJ disruption was restored following treatment with HDAC6 inhibitors (Figs. 5 and 6). However, the molecular mechanisms by which GARS regulates NMJ formation and function and how HDAC6 inhibitors directly affect GARS in NMJs remain unclear. Indeed, the function of GARS in the regulation of HDAC6 activity remains unclear. Although previous reports have suggested a gain-of-function effect of several mutant forms of *GARS* with respect to HDAC6 activity (Mo et al., 2018), other data have shown that WT GARS interacts with HDAC6 to inhibit the deacetylation of α-tubulin and knockdown of *GARS* activates HDAC6 (Mo et al., 2018). Moreover, treatment with HDAC6 inhibitors affects the acetylation of α-tubulin in *Gars*-mutant mice with CMT phenotypes (Mo et al., 2018). Consistently, in zebrafish model, *gars* depletion led to a decrease in α-tubulin acetylation and disruption of NMJ formation (Holloway et al., 2016). Therefore, these data suggest that GARS affects the activity of HDAC6 by regulating its expression or binding to HDAC6. Therefore, further studies are needed to understand the mechanism by which GARS regulates HDAC6 activation will follow. In addition, our data, which showed the significant recovery of NMJ defects following treatment with pan-HDAC inhibitors, suggest that not only HDAC6 but also other HDACs may be involved in GARS-dependent NMJ development. Therefore, further studies are needed to determine whether GARS modulates microtubule dynamics in muscle cells and/or neurons through microtubule acetylation and whether the GARS-dependent microtubule stability of these cells is related to NMJ formation/function.

CKD-504, a hydroxybenzamide HDAC6 inhibitor that chelates Zn^{2+}, has emerged as an attractive therapeutic agent for Huntington's disease (HD) and CMT (Ha et al., 2020). The advantages of CKD-504 include its high enzymatic activity and selectivity for HDAC6 (Ha et al., 2020). Intracellular transport along the microtubules in motor neurons is important for axonal guidance via the NMJ to muscle cells (Banerjee and Riordan, 2018; Vilmont et al., 2016), and HDAC6 is a negative regulator of intracellular transport (Valenzuela-Fernandez et al., 2008; Wenzel et al., 2019). A previous study suggested that HDAC6 inhibitors used in the treatment of HD act on mechanisms to enhance the intracellular transport of brain-derive neurotrophic factor and increase microtubule acetylation (Dompierre et al., 2007). Individuals with CMT exhibiting mutations in *GARS* present with motility deficits

induced by impaired axonal guidance and neuronal degeneration (He et al., 2015; Sleigh et al., 2020). In the present study, we showed that CKD-504 was sufficient to repair NMJ defects and motility disruptions exhibited in a *gars*-KD zebrafish model. Although our data suggest that the recovery of NMJs following treatment with CKD-504, an HDAC6 inhibitor, may be a novel therapeutic approach for the treatment of CMTs, it is unclear whether this effect has the NMJ as the primary target. Therefore, future studies are needed to elucidate the molecular mechanisms by which CKD-504 restores NMJ defects using more NMJ-related disease models.

Note: Supplementary information is available on the Molecules and Cells website (www.molcells.org).

ACKNOWLEDGMENTS

This work was supported by the National Research Foundation, funded by the Korean government's MSIP (2021R1A2C3004572 to J.E.L., 2021R1A6A3A13041249 to H.S.J., 2021R1A4A2001389 to K.W.C., B.O.C., and J.E.L.), and was supported by the National Institutes of Health, USA (NIH RO1 NS094388 to B.O.C. and D.H.K.).

AUTHOR CONTRIBUTIONS

H.S.J. conducted the experiments and analyzed the data with substantial contributions from H.J.K., D.H.K., K.W.C., and B.O.C. who advised the experimental designs and commented on the manuscript. J.E.L. designed the experiments and wrote the manuscript with substantial contributions from H.S.J. and B.O.C.

CONFLICTS OF INTEREST

D.H.K. is a scientific founder and equity holder of Curi Bio. The other authors have no potential conflicts of interest to disclose.

ORCID

Hui Su Jeong	https://orcid.org/0000-0001-8419-4698
Hye Jin Kim	https://orcid.org/0000-0002-7636-3639
Deok-Ho Kim	https://orcid.org/0000-0002-6989-6074
Ki Wha Chung	https://orcid.org/0000-0003-0363-8432
Byung-Ok Choi	https://orcid.org/0000-0001-5459-1772
Ji Eun Lee	https://orcid.org/0000-0002-4898-741X

REFERENCES

Antonellis, A., Ellsworth, R.E., Sambuughin, N., Puls, I., Abel, A., Lee-Lin, S.Q., Jordanova, A., Kremensky, I., Christodoulou, K., Middleton, L.T., et al. (2003). Glycyl tRNA synthetase mutations in Charcot-Marie-Tooth disease type 2D and distal spinal muscular atrophy type V. Am. J. Hum. Genet. *72*, 1293-1299.

Antonellis, A., Lee-Lin, S.Q., Wasterlain, A., Leo, P., Quezado, M., Goldfarb, L.G., Myung, K., Burgess, S., Fischbeck, K.H., and Green, E.D. (2006). Functional analyses of glycyl-tRNA synthetase mutations suggest a key role for tRNA-charging enzymes in peripheral axons. J. Neurosci. *26*, 10397-10406.

Asthana, J., Kapoor, S., Mohan, R., and Panda, D. (2013). Inhibition of HDAC6 deacetylase activity increases its binding with microtubules and suppresses microtubule dynamic instability in MCF-7 cells. J. Biol. Chem. *288*, 22516-22526.

Banerjee, S. and Riordan, M. (2018). Coordinated regulation of axonal microtubule organization and transport by *Drosophila* neurexin and BMP pathway. Sci. Rep. *8*, 17337.

Benoy, V., Van Helleputte, L., Prior, R., d'Ydewalle, C., Haeck, W., Geens, N., Scheveneels, W., Schevenels, B., Cader, M.Z., Talbot, K., et al. (2018). HDAC6 is a therapeutic target in mutant GARS-induced Charcot-Marie-Tooth disease. Brain *141*, 673-687.

Borg, K. and Ericson-Gripenstedt, U. (2002). Muscle biopsy abnormalities differ between Charcot-Marie-Tooth type 1 and 2: reflect different pathophysiology? Exerc. Sport Sci. Rev. *30*, 4-7.

Bremer, J., Skinner, J., and Granato, M. (2017). A small molecule screen identifies *in vivo* modulators of peripheral nerve regeneration in zebrafish. PLoS One *12*, e0178854.

Butler, K.V., Kalin, J., Brochier, C., Vistoli, G., Langley, B., and Kozikowski, A.P. (2010). Rational design and simple chemistry yield a superior, neuroprotective HDAC6 inhibitor, tubastatin A. J. Am. Chem. Soc. *132*, 10842-10846.

Chapela, D., Sousa, S., Martins, I., Cristovao, A.M., Pinto, P., Corte-Real, S., and Saude, L. (2019). A zebrafish drug screening platform boosts the discovery of novel therapeutics for spinal cord injury in mammals. Sci. Rep. *9*, 10475.

Chen, S., Owens, G.C., Makarenkova, H., and Edelman, D.B. (2010). HDAC6 regulates mitochondrial transport in hippocampal neurons. PLoS One *5*, e10848.

Choi, H., Kim, H.J., Yang, J., Chae, S., Lee, W., Chung, S., Kim, J., Choi, H., Song, H., Lee, C.K., et al. (2020). Acetylation changes tau interactome to degrade tau in Alzheimer's disease animal and organoid models. Aging Cell *19*, e13081.

Cirrincione, A.M., Pellegrini, A.D., Dominy, J.R., Benjamin, M.E., Utkina-Sosunova, I., Lotti, F., Jergova, S., Sagen, J., and Rieger, S. (2020). Paclitaxel-induced peripheral neuropathy is caused by epidermal ROS and mitochondrial damage through conserved MMP-13 activation. Sci. Rep. *10*, 3970.

Cirrincione, A.M. and Rieger, S. (2020). Analyzing chemotherapy-induced peripheral neuropathy *in vivo* using non-mammalian animal models. Exp. Neurol. *323*, 113090.

Dompierre, J.P., Godin, J.D., Charrin, B.C., Cordelieres, F.P., King, S.J., Humbert, S., and Saudou, F. (2007). Histone deacetylase 6 inhibition compensates for the transport deficit in Huntington's disease by increasing tubulin acetylation. J. Neurosci. *27*, 3571-3583.

d'Ydewalle, C., Krishnan, J., Chiheb, D.M., Van Damme, P., Irobi, J., Kozikowski, A.P., Vanden Berghe, P., Timmerman, V., Robberecht, W., and Van Den Bosch, L. (2011). HDAC6 inhibitors reverse axonal loss in a mouse model of mutant HSPB1-induced Charcot-Marie-Tooth disease. Nat. Med. *17*, 968-974.

Ennerfelt, H., Voithofer, G., Tibbo, M., Miller, D., Warfield, R., Allen, S., and Kennett Clark, J. (2019). Disruption of peripheral nerve development in a zebrafish model of hyperglycemia. J. Neurophysiol. *122*, 862-871.

Grice, S.J., Sleigh, J.N., Motley, W.W., Liu, J.L., Burgess, R.W., Talbot, K., and Cader, M.Z. (2015). Dominant, toxic gain-of-function mutations in *gars* lead to non-cell autonomous neuropathology. Hum. Mol. Genet. *24*, 4397-4406.

Ha, N., Choi, Y.I., Jung, N., Song, J.Y., Bae, D.K., Kim, M.C., Lee, Y.J., Song, H., Kwak, G., Jeong, S., et al. (2020). A novel histone deacetylase 6 inhibitor improves myelination of Schwann cells in a model of Charcot-Marie-Tooth disease type 1A. Br. J. Pharmacol. *177*, 5096-5113.

He, W., Bai, G., Zhou, H., Wei, N., White, N.M., Lauer, J., Liu, H., Shi, Y., Dumitru, C.D., Lettieri, K., et al. (2015). CMT2D neuropathy is linked to the neomorphic binding activity of glycyl-tRNA synthetase. Nature *526*, 710-714.

Holloway, M.P., DeNardo, B.D., Phornphutkul, C., Nguyen, K., Davis, C., Jackson, C., Richendrfer, H., Creton, R., and Altura, R.A. (2016). An

asymptomatic mutation complicating severe chemotherapy-induced peripheral neuropathy (CIPN): a case for personalised medicine and a zebrafish model of CIPN. NPJ Genom. Med. *1*, 16016.

Howard, J.F., Jr. (2018). Myasthenia gravis: the role of complement at the neuromuscular junction. Ann. N. Y. Acad. Sci. *1412*, 113-128.

Janke, C. and Bulinski, J.C. (2011). Post-translational regulation of the microtubule cytoskeleton: mechanisms and functions. Nat. Rev. Mol. Cell Biol. *12*, 773-786.

Jung, J., Choi, I., Ro, H., Huh, T.L., Choe, J., and Rhee, M. (2020). *march5* governs the convergence and extension movement for organization of the telencephalon and diencephalon in zebrafish embryos. Mol. Cells *43*, 76-85.

Kalebic, N., Martinez, C., Perlas, E., Hublitz, P., Bilbao-Cortes, D., Fiedorczuk, K., Andolfo, A., and Heppenstall, P.A. (2013). Tubulin acetyltransferase alphaTAT1 destabilizes microtubules independently of its acetylation activity. Mol. Cell. Biol. *33*, 1114-1123.

Kesner, V.G., Oh, S.J., Dimachkie, M.M., and Barohn, R.J. (2018). Lambert-Eaton myasthenic syndrome. Neurol. Clin. *36*, 379-394.

Lee, H.J., Park, J., Nakhro, K., Park, J.M., Hur, Y.M., Choi, B.O., and Chung, K.W. (2012). Two novel mutations of GARS in Korean families with distal hereditary motor neuropathy type V. J. Peripher. Nerv. Syst. *17*, 418-421.

Licciardi, P.V. and Karagiannis, T.C. (2012). Regulation of immune responses by histone deacetylase inhibitors. ISRN Hematol. *2012*, 690901.

Loprest, L.J., Pericak-Vance, M.A., Stajich, J., Gaskell, P.C., Lucas, A.M., Lennon, F., Yamaoka, L.H., Roses, A.D., and Vance, J.M. (1992). Linkage studies in Charcot-Marie-Tooth disease type 2: evidence that CMT types 1 and 2 are distinct genetic entities. Neurology 42(3 Pt 1), 597-601.

Mann, B.S., Johnson, J.R., Cohen, M.H., Justice, R., and Pazdur, R. (2007). FDA approval summary: vorinostat for treatment of advanced primary cutaneous T-cell lymphoma. Oncologist *12*, 1247-1252.

Mariadason, J.M. (2008). HDACs and HDAC inhibitors in colon cancer. Epigenetics *3*, 28-37.

Menelaou, E., Husbands, E.E., Pollet, R.G., Coutts, C.A., Ali, D.W., and Svoboda, K.R. (2008). Embryonic motor activity and implications for regulating motoneuron axonal pathfinding in zebrafish. Eur. J. Neurosci. *28*, 1080-1096.

Mo, Z., Zhao, X., Liu, H., Hu, Q., Chen, X.Q., Pham, J., Wei, N., Liu, Z., Zhou, J., Burgess, R.W., et al. (2018). Aberrant GlyRS-HDAC6 interaction linked to axonal transport deficits in Charcot-Marie-Tooth neuropathy. Nat. Commun. *9*, 1007.

Morena, J., Gupta, A., and Hoyle, J.C. (2019). Charcot-Marie-Tooth: from molecules to therapy. Int. J. Mol. Sci. *20*, 3419.

Namdar, M., Perez, G., Ngo, L., and Marks, P.A. (2010). Selective inhibition of histone deacetylase 6 (HDAC6) induces DNA damage and sensitizes transformed cells to anticancer agents. Proc. Natl. Acad. Sci. U. S. A. *107*, 20003-20008.

Niehues, S., Bussmann, J., Steffes, G., Erdmann, I., Kohrer, C., Sun, L., Wagner, M., Schafer, K., Wang, G., Koerdt, S.N., et al. (2015). Impaired protein translation in Drosophila models for Charcot-Marie-Tooth neuropathy caused by mutant tRNA synthetases. Nat. Commun. *6*, 7520.

Osseni, A., Ravel-Chapuis, A., Thomas, J.L., Gache, V., Schaeffer, L., and Jasmin, B.J. (2020). HDAC6 regulates microtubule stability and clustering of AChRs at neuromuscular junctions. J. Cell Biol. *219*, e201901099.

Ponomareva, O.Y., Eliceiri, K.W., and Halloran, M.C. (2016). Charcot-Marie-Tooth 2b associated Rab7 mutations cause axon growth and guidance defects during vertebrate sensory neuron development. Neural Dev. *11*, 2.

Rodriguez Cruz, P.M., Cossins, J., Beeson, D., and Vincent, A. (2020). The neuromuscular junction in health and disease: molecular mechanisms governing synaptic formation and homeostasis. Front. Mol. Neurosci. *13*, 610964.

Seburn, K.L., Nangle, L.A., Cox, G.A., Schimmel, P., and Burgess, R.W. (2006). An active dominant mutation of glycyl-tRNA synthetase causes neuropathy in a Charcot-Marie-Tooth 2D mouse model. Neuron *51*, 715-726.

Simoes-Pires, C., Zwick, V., Nurisso, A., Schenker, E., Carrupt, P.A., and Cuendet, M. (2013). HDAC6 as a target for neurodegenerative diseases: what makes it different from the other HDACs? Mol. Neurodegener. *8*, 7.

Sivakumar, K., Kyriakides, T., Puls, I., Nicholson, G.A., Funalot, B., Antonellis, A., Sambuughin, N., Christodoulou, K., Beggs, J.L., Zamba-Papanicolaou, E., et al. (2005). Phenotypic spectrum of disorders associated with glycyl-tRNA synthetase mutations. Brain *128*, 2304-2314.

Sleigh, J.N., Dawes, J.M., West, S.J., Wei, N., Spaulding, E.L., Gomez-Martin, A., Zhang, Q., Burgess, R.W., Cader, M.Z., Talbot, K., et al. (2017). Trk receptor signaling and sensory neuron fate are perturbed in human neuropathy caused by *Gars* mutations. Proc. Natl. Acad. Sci. U. S. A. *114*, E3324-E3333.

Sleigh, J.N., Grice, S.J., Burgess, R.W., Talbot, K., and Cader, M.Z. (2014). Neuromuscular junction maturation defects precede impaired lower motor neuron connectivity in Charcot-Marie-Tooth type 2D mice. Hum. Mol. Genet. *23*, 2639-2650.

Sleigh, J.N., Mech, A.M., and Schiavo, G. (2020). Developmental demands contribute to early neuromuscular degeneration in CMT2D mice. Cell Death Dis. *11*, 564.

Smith, A., Kim, J.H., Chun, C., Gharai, A., Moon, H.W., Kim, E.Y., Nam, S.H., Ha, N., Song, J.Y., Chung, K.W., et al. (2022). HDAC6 inhibition corrects electrophysiological and axonal transport deficits in a human stem cell-based model of Charcot-Marie-Tooth disease (type 2D). Adv. Biol. (Weinh.) *6*, e2101308.

Son, I.H., Chung, I.M., Lee, S.I., Yang, H.D., and Moon, H.I. (2007). Pomiferin, histone deacetylase inhibitor isolated from the fruits of Maclura pomifera. Bioorg. Med. Chem. Lett. *17*, 4753-4755.

Valenzuela-Fernandez, A., Cabrero, J.R., Serrador, J.M., and Sanchez-Madrid, F. (2008). HDAC6: a key regulator of cytoskeleton, cell migration and cell-cell interactions. Trends Cell Biol. *18*, 291-297.

Vilmont, V., Cadot, B., Vezin, E., Le Grand, F., and Gomes, E.R. (2016). Dynein disruption perturbs post-synaptic components and contributes to impaired MuSK clustering at the NMJ: implication in ALS. Sci. Rep. *6*, 27804.

Wenzel, E.D., Speidell, A., Flowers, S.A., Wu, C., Avdoshina, V., and Mocchetti, I. (2019). Histone deacetylase 6 inhibition rescues axonal transport impairments and prevents the neurotoxicity of HIV-1 envelope protein gp120. Cell Death Dis. *10*, 674.

Wong, V.S.C., Picci, C., Swift, M., Levinson, M., Willis, D., and Langley, B. (2018). alpha-tubulin acetyltransferase is a novel target mediating neurite growth inhibitory effects of chondroitin sulfate proteoglycans and myelin-associated glycoprotein. eNeuro *5*, ENEURO.0240-17.2018.

Zhang, Y., Li, N., Caron, C., Matthias, G., Hess, D., Khochbin, S., and Matthias, P. (2003). HDAC-6 interacts with and deacetylates tubulin and microtubules in vivo. EMBO J. *22*, 1168-1179.